# Role of spacer cations and structural distortion in two-dimensional germanium halide perovskites

Rossella Chiara,[a] Marta Morana,*[a] Massimo Boiocchi,[b] Mauro Coduri,[a] Marinella Striccoli,[c] Francesco Fracassi,[c] Andrea Listorti,[c] Arup Mahata,[de] Paolo Quadrelli,[a] Mattia Gaboardi,[f] Chiara Milanese,[a] Luca Bindi,[g] Filippo De Angelis[deh] and Lorenzo Malavasi*[a]

*Corresponding authors

[a]Department of Chemistry and INSTM, University of Pavia, Via Taramelli 16, Pavia, Italy
**E-mail:** marta.morana@universitadipavia.it, lorenzo.malavasi@unipv.it
**Tel:** +39 382 987921

[b]Centro Grandi Strumenti (CGS), University of Pavia, Via Bassi 21, Pavia, Italy

[c]Department of Chemistry, University of Bari "Aldo Moro", Via Orabona 4, Bari, Italy

[d]Computational Laboratory for Hybrid/Organic Photovoltaics (CLHYO), Istituto CNR di Scienze e Tecnologie Chimiche "Giulio Natta" (CNR-SCITEC), Via Elce di Sotto 8, 06123 Perugia, Italy

[e]CompuNet, Istituto Italiano di Tecnologia, Via Morego 30, 16163 Genova, Italy

[f]Elettra-Sincrotrone Trieste S. C. p. A., S.S. 14 km 163.5 in Area Science Park, Basovizza, Trieste, Italy

[g]Dipartimento di Scienze della Terra, Università degli Studi di Firenze, Via G. La Pira 4, 50121 Firenze, Italy

[h]Department of Chemistry, Biology and Biotechnology, University of Perugia, Via Elce di Sotto 8, 06123 Perugia, Italy

**Abstract**

The elucidation of the structure–property correlation in 2D metal halide perovskite is a key issue to understand the dependence of optical properties on structural distortions and to design novel tailored materials. To extend the actual knowledge on this kind of correlation for lead-free materials, here we report four novel 2D germanium bromide perovskites, namely $A_2GeBr_4$ with A = phenylethylammonium, PEA, Br-phenylethylammonium, BrPEA, F-phenylethylammonium, FPEA, and benzylammonium BZA. A dependence of the band gap value and emission characteristics in terms of Stokes shift and peak width has been highlighted and correlated with the octahedral distortion parameters. In addition, by comparing the actual results with previous data on analogous Sn- and Pb-based materials, we observed an intrinsic increased distortion induced by germanium, particularly on the octahedral bond elongation and bond angle variance, and less on the Ge–Br–Ge bond angle. The structural and optical investigation, together with density functional theory simulations, clarified the role of different structural distortion parameters on the optical properties for a series of 2D Ge-containing perovskites, thus providing novel clues for the future design of layered lead-free materials.

## Introduction

Two-dimensional (2D) metal halide perovskites (MHPs) are attracting increasing interest in the science/energy community thanks to their vast structural/compositional diversity, which allows tuning of their properties by playing with the cage and spacer cations.[1–4] Among the different structural classes of 2D perovskites, the Ruddlesden–Popper (RP) phases of general formula $A_2'A_{n-1}B_nX_{3n+1}$ (where A' = spacer cation, A = small cation, B = metal and X = halide) are extensively investigated owing to their ability to accommodate a plethora of organic spacers, allowing the study of quantum-confinement effects by modulating the *n*-layer thickness *via* simple synthetic chemistry.[1] The vast chemical tunability of 2D MHPs has triggered significant interest in the elucidation of the role of crystal structure, the nature of the organic cation, and structural deformations on the optical properties of these materials.[1,2,5–9] This aim, together with the desire for playing with the chemical and structural degrees of freedom of 2D perovskites, has led to the continuous preparation and characterization of novel materials, thus enlarging the material records and providing reliable correlations. So far, the number of spacers investigated, considering both mono- and di-amines, has been significant leading to the extension of 2D MHPs to several structural families in addition to the well-known RP and Dion–Jacobson (DJ) categories.[1–4]

Coming to the cage cation, *i.e.* the metal ion, nearly all of the available reports on 2D perovskites have focused on lead-based and more recently tin-based phases. As a matter of fact, the initial input in developing two-dimensional MHPs originated from their possible use in the 2D/3D bi-layered structure to improve the efficiency and stability of lead halide perovskite solar cells (PSCs).[10] Starting from this photovoltaics exploitation, the interest around 2D perovskites has grown significantly, leading to their possible use in various fields of application such as for light-emitting devices (LEDs), where their performances can surpass those of 3D perovskites, as well as in more emerging fields such as lasing and photodetection.[11–17]

This interest comes from the unique optical properties of 2D halide perovskites where the confinement of the charge carriers in the inorganic layers leads, in general, to large excitonic binding energies with respect to 3D perovskites, and narrow-band photoluminescence (PL).[1,5] However, the modulation of the organic spacer can significantly tune the PL emission to broadband as a consequence of the octahedral distortion induced by hydrogen bonding, thus modifying the tendency for charge trapping.[5,18–22] Analogously, the band gap ($E_g$) of 2D perovskites can be modified by adjusting the angular distortion between adjacent metal-halide octahedra, with an increase of the $E_g$ as the angle deviates progressively from 180°.[6,7,9] By playing with the size of the organic ammonium cation, the extent and direction of the inorganic octahedral framework distortion can be modulated, having a different impact on band structure and therefore on the band gap.[6]

So far, the correlation between structural distortion and the band gap in 2D lead- and tin-containing perovskites has proved to be solid, thanks to the high and diverse number of prepared compositions, highlighting the impact of the interlayer metal (M) distance (or squared value), the average X–M–X (X = halogen) bond angle, average M–X bond length, as well as the octahedral volume.[6,9] Much less has been done for alternative lead-free MHPs that incorporate other suitable metals, such as Ge, Bi, and Sb.[23,24] In this respect, germanium is a fascinating alternative belonging to the same group of Sn and Pb, being Earth-abundant and with comparatively little toxicity or environmental concerns, thereby overcoming a major drawback of Pb-based perovskites.[42] With respect to 2D Ge-containing halide perovskites with *n* = 1, just a couple of experimental reports are available in the current literature, namely, on $BA_2GeBr_4$ and $PEA_2GeI_4$.[25–27] Both compositions show quite wide PL emissions centered, respectively, at ~450 nm and ~630 nm.[25,27] However, the very limited number of available phases, containing also different halides, hinders any possible correlation between structural distortions and the optical properties. We believe that owing to the increasing interest in Ge-based materials, and to the fascinating properties and modulation routes provided by 2D perovskites, enlarging the group of such phases may help in designing novel materials and also in

extending the actual knowledge about the correlation between the crystal structure details and optical properties. For these reasons, we synthesized and characterized four novel RP 2D germanium bromide perovskites ($n$ = 1), namely $A_2GeBr_4$ with A = $C_6H_4CH_2CH_2NH_3$ (phenylethylammonium, PEA), $BrC_6H_4CH_2CH_2NH_3$ (Br-phenylethylammonium, BrPEA), $FC_6H_4CH_2CH_2NH_3$ (F-phenylethylammonium, FPEA), and $C_6H_4CH_2NH_3$ (benzylammonium BZA). The chemical formula of the four organic cations is reported in Fig. 1. The crystal structure and phase behavior of these novel compounds were determined using single-crystal X-ray diffraction (SCXRD) and variable temperature synchrotron X-ray powder diffraction (SXRPD) techniques, while the optical properties were investigated by absorption spectroscopy and steady-state and time-resolved PL in an effort to unveil a possible correlation between the band gap and emission properties with structural features, as already done for Pb and Sn analogues.[6,9]

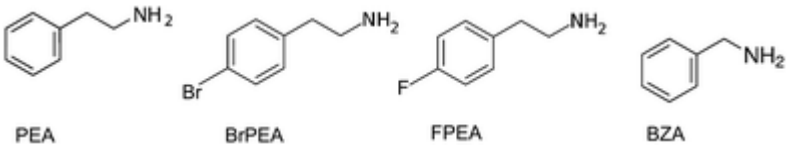


**Fig. 1** Chemical formulae of the four amines used to prepare the Ge-based 2D perovskites: PEA, BrPEA, FPEA, and BZA.

Samples were grown by solution chemistry as described in the Experimental section (ESI†) while photos of the crystals are reported in Fig. S1 (ESI†). SCXRD revealed that the four investigated structures consist of a single 〈100〉-oriented layer of $GeBr_6$ octahedra alternating with organic cation bilayers, and the corresponding structural sketches are reported in Fig. 2.[28]

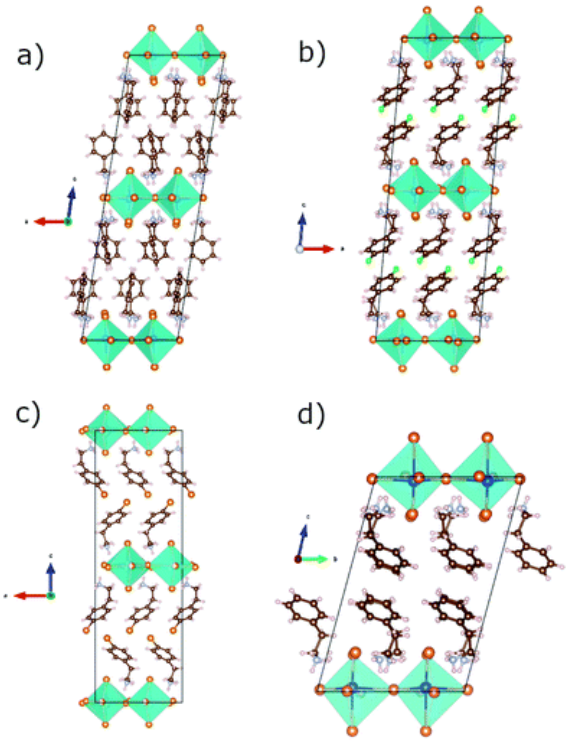


**Fig. 2** Structural sketches of (a) $PEA_2GeBr_4$, (b) $FPEA_2GeBr_4$, (c) $BrPEA_2GeBr_4$ and (d) $BZA_2GeBr_4$.

The crystal symmetry ranges from triclinic to orthorhombic, as reported in Table 1, with $PEA_2GeBr_4$ and $BZA_2GeBr_4$ crystallizing in space group $P\bar{1}$, and $FPEA_2GeBr_4$ and $BrPEA_2GeBr_4$ crystallizing in $P2_1/n$ and $Pna2_1$, respectively.

**Table 1** Structural parameters of $PEA_2GeBr_4$, $FPEA_2GeBr_4$, $BrPEA_2GeBr_4$ and $BZA_2GeBr_4$

| Sample | Chemical formula | Space group and lattice volume ($Å^3$) | Lattice parameters (Å) | Bond angles (°) |
|---|---|---|---|---|
| $PEA_2GeBr_4$ | $(C_6H_4CH_2CH_2NH_3)_2GeBr_4$ | $P\bar{1}$ | 11.4059(12) | 80.5161(14) |
| | | 2181.4(4) | 11.5242(12) | 74.9498(14) |
| | | | 17.4408(19) | 90.0119(14) |
| $BrPEA_2GeBr_4$ | $(BrC_6H_4CH_2CH_2NH_3)_2GeBr_4$ | $Pna2_1$ | 11.3957(12) | 90 |
| | | 2347.1(4) | 5.7978(6) | 90 |
| | | | 35.524(4) | 90 |
| $FPEA_2GeBr_4$ | $(FC_6H_4CH_2CH_2NH_3)_2GeBr_4$ | $P2_1/n$ | 33.5176(12) | 90 |
| | | 4375.9(2) | 11.5028(3) | 94.990(3) |
| | | | 11.3930(3) | 90 |
| $BZA_2GeBr_4$ | $(C_6H_4CH_2NH_3)_2GeBr_4$ | $P\bar{1}$ | 11.1707(16) | 99.569(4) |
| | | 4245.0(10) | 11.4313(16) | 99.275(2) |
| | | | 34.172(5) | 90.012(2) |

According to the above discussion, we used the structural data obtained to extract some relevant parameters correlating with the structural distortions.[5,6,29] The distortion of the octahedra themselves can be quantified in terms of the average octahedral elongation length ( $\langle\lambda_{oct}\rangle$ ) and their bond angle variance ($\sigma_{oct}^2$), as defined by Robinson *et al.*, and is usually related to a broadened photoluminescence.[5,30] The distortion increases from $BZA_2GeBr_4$ to the PEA-containing samples, reaching a maximum for $BrPEA_2GeBr_4$ (Fig. 3); it is worth noting that $BrPEA_2GeBr_4$ shows the splitting of the Ge and of two Br crystallographic sites, which might cause a larger distortion.

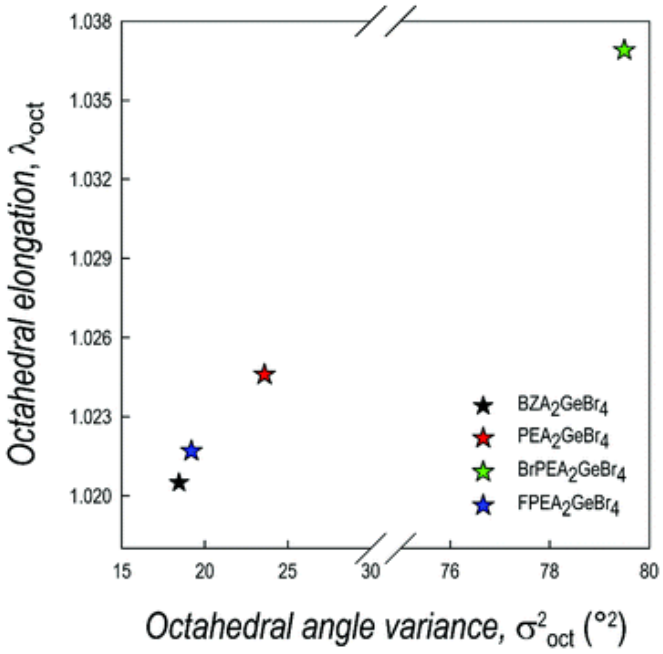


**Fig. 3** Octahedral distortion parameters for $PEA_2GeBr_4$, $BrPEA_2GeBr_4$, $FPEA_2GeBr_4$ and $BZA_2GeBr_4$.

This trend is consistent with previous examples referring to Sn- and Pb-based 2D perovskites reported in the literature (Fig. S2, ESI†), where $BZA_2MBr_4$ compounds (M = Pb, Sn) show small distortion parameters, and $PEA_2PbBr_4$ has a larger structural strain.

The presence of Ge seems to deeply affect the distortion within the octahedra. For example, in the case of the BZA organic spacer, the Ge–Br bond length varies from 2.5555(12) to 3.3279(15) Å, while the M–Br length ranges from 2.972(3) to 2.9959(11) Å in $BZA_2PbBr_4$ and from 2.940(4) to 2.977(1) Å in $BZA_2SnBr_4$.[29,31] Furthermore, a distortion index of the bond length of 0.1185 is larger than the values of 0.0039 and 0.0031 reported for $BZA_2SnBr_4$ and $BZA_2PbBr_4$, respectively, and, consistently, the octahedral elongation increases from the value of 1.000 of $BZA_2SnBr_4$ and $BZA_2PbBr_4$ to 1.0202.[29,31] Analogously, the octahedral angle variance of $BZA_2GeBr_4$ is two orders of magnitude larger with respect to $BZA_2SnBr_4$ and $BZA_2PbBr_4$.[31] Considering the compounds containing PEA, which generally show the largest distortion, we observe a similar structural strain induced by Ge. In fact, the Pb-containing analogue has the mean equatorial and axial bond lengths of 3.0018 and 3.0372 Å, respectively, a quadratic elongation of 1.0056 and an octahedral angle variance of 16.3496, while the Sn-containing sample has an average bond length of 3.0070 Å, from 2.8515(9) to 3.1744(9) Å, a quadratic elongation of 1.0058 and an angle variance of 17.3527.[29,32] Comparing these parameters with the respective values of 2.9365 Å, ranging from 2.5377(12) to 3.3532(14) Å, 1.0245 and 23.5846 in the Ge samples, it is clear that the octahedra are less regular and more distorted.

On the other hand, the presence of Ge has a smaller effect on the distortion between adjacent octahedra, which can be quantified as the deviation of the angle between the octahedra from 180°. In fact, for BZA the M–Br–M angle increases from 149.96° for Pb to 152° for Sn and 155.27° for Ge.[29,31] Analogously, for samples containing PEA, the angle increases from 151.46° for Pb to 152.54° for Sn and 157.82° for Ge.[29,31] Notably, the reported Ge–I–Ge angle in $PEA_2GeI_4$ is 158.34°, suggesting that the presence of Ge might induce a smaller distortion of the inorganic layers.[27] The distortion parameters for the four novel Ge-based 2D perovskites are summarized in Table S1 (ESI†) and will in the following be used to discuss a possible correlation with the optical properties presented below.

The possible phase transitions and the phase stability of the $PEA_2GeBr_4$, $BrPEA_2GeBr_4$, $FPEA_2GeBr_4$, and $BZA_2GeBr_4$ samples have been checked by means of differential scanning calorimetry (DSC) and variable-temperature SXRPD. Fig. 4a shows the DSC traces of the samples between −75 and 75 °C, and these are flat, confirming the absence of peaks related to structural transitions. The low-*T* diffraction data have been refined using the RT SCXRD data, confirming the validity of the RT crystal structures to fit the patterns in the whole temperature range. The trend of the lattice volume as a function of temperature, as determined by Rietveld refinement (representative fits in Fig. S3, ESI†) for the four samples, is presented in Fig. 4b and shows the expected progressive contraction of *V* upon reducing the temperature. As a further test, single crystals of $PEA_2GeBr_4$, $FPEA_2GeBr_4$, and $BZA_2GeBr_4$ were selected and characterized by SCXRD at 100 K. The compounds crystallize in the same structure, owing to the expected reduction in cell parameters and contraction of the bond lengths and the distortion parameters (see Table S2, ESI†).

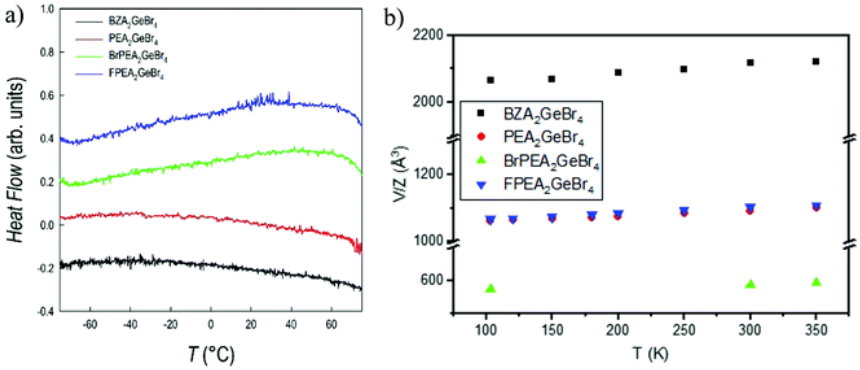


**Fig. 4** (a) DSC traces and, (b) trend of lattice volume as a function of temperature for $PEA_2GeBr_4$, $BrPEA_2GeBr_4$, $FPEA_2GeBr_4$ and $BZA_2GeBr_4$.

Fig. 5a and b report the comparison among the normalized absorption and PL spectra for PEA2GeBr4, BrPEA2GeBr4, FPEA2GeBr4, and BZA2GeBr4, while Fig. 5c and d show the PL recombination dynamics measured by TCSPC.

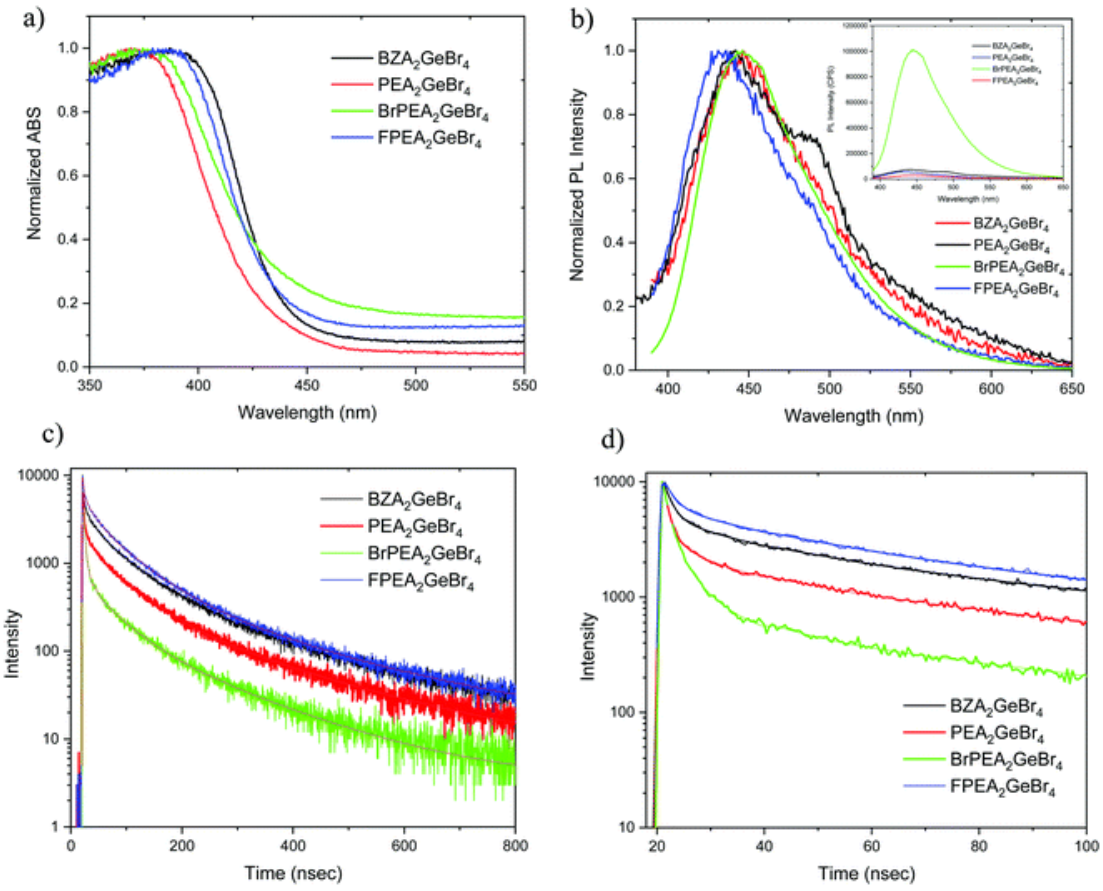


**Fig. 5** (a) Normalized optical absorbance and (b) steady-state PL ($\lambda_{exc}$ = 370 nm) and (c and d) TR decay profiles of $PEA_2GeBr_4$, $BrPEA_2GeBr_4$, $FPEA_2GeBr_4$ and $BZA_2GeBr_4$ ($\lambda_{exc}$ = 375 nm). The fitting curves are reported as solid lines in the decay measurements. The non-normalized PL spectra are shown in the inset of (b).

The band gap of the samples was determined from Tauc plots by considering a direct band gap nature, as determined by DFT calculations (see later in the text), and corresponds to 3.01 eV for $PEA_2GeBr_4$, 2.95 eV for $BrPEA_2GeBr_4$, 2.91 eV for $FPEA_2GeBr_4$, and 2.89 eV $BZA_2GeBr_4$ (see Fig. S4, ESI†). PL data confirm the variation of the band gap along with the change of the organic spacer, with the emission band peaking at 2.78 eV for both $PEA_2GeBr_4$ and $BrPEA_2GeBr_4$, 2.85 eV for $FPEA_2GeBr_4$, and 2.81 eV for $BZA_2GeBr_4$. The Stokes shift is not uniform across the samples, with $FPEA_2GeBr_4$ and $BZA_2GeBr_4$ showing a smaller shift of about 0.3 eV, and $PEA_2GeBr_4$ and $BrPEA_2GeBr_4$ a larger one of about 0.46 eV. The comparison of the PL spectra in the inset of Fig. 5b highlights the intense emission of $BrPEA_2GeBr_4$ with respect to the other $GeBr_4$ samples, generally characterized by a moderate PL intensity. The normalized PL spectra show clearly that the emission bands are relatively broad, in comparison to the 2D lead-based perovskites, due to the above discussed structural distortions, showing a full width at half maximum (FWHM) that varies from 0.5 eV for the narrower $BrPEA_2GeBr_4$, to 0.65 eV of the wider $BZA_2GeBr_4$, with the central member of the series having an FWHM of about 0.6 eV.[5] The $BZA_2GeBr_4$ emission also shows some hints of band structuring, with a weak shoulder appearing at lower energies. The time-resolved PL (TRPL) spectra in Fig. 5c and d show the decay profiles for all the samples. While analogue recombination dynamics are observed for $BZA_2GeBr_4$ and $FPEA_2GeBr_4$, characterized also by very similar band gaps and Stokes shift values, the decay becomes shorter for $PEA_2GeBr_4$ and more significantly for $BrPEA_2GeBr_4$, the latter also being characterized by a considerable fluorescence enhancement. The average lifetimes are calculated by fitting the PL decay with multi-exponential functions, carrying out decay profile interpolations using the least squares method. A $\tau_{average}$ of

about 113 ns is calculated for $BZA_2GeBr_4$ and of 109 ns for $FPEA_2GeBr_4$, while a slightly more rapid lifetime of 102 ns is obtained for $PEA_2GeBr_4$ that significantly decreases to about 68 ns for $BrPEA_2GeBr_4$. The latter shows therefore the most intense emission and the shortest lifetime.[33] From Fig. 5d we note how the difference in lifetimes among the four 2D germanium bromide perovskites is mainly determined within the first 30 ns, and is therefore significantly influenced by the excitonic recombination mechanisms.

The band gap evolution of the systems was also investigated using density functional theory (DFT) calculations. The difference in absolute band gap value between theory and experiment is due to the exciton binding energy, which is not included in our calculations. Generally, such thin quantum well two-dimensional perovskites possess a high exciton binding energy in the range of ~300–450 meV, thus considering such exciton binding energy values, our experimental and theoretical band gap converges nicely.[34,35] While looking at the bandgap evolution among $PEA_2GeBr_4$ and its halogen substituents, $PEA_2GeBr_4$ shows the highest band gap, followed by a subsequent decrease in the bandgap with Br- and F-substitution at the PEA cation, which is very similar to experiment. A direct band gap comparison between $BZA_2GeBr_4$ and its halogen-substituted analogues is not possible due to the presence of the halogen substituents which introduce a fundamental difference by forming better stacking in the organic layers and hydrogen bonding in the structure.[36] In fact, it has already been reported that the stacking difference and hydrogen bonding can change the electronic properties significantly in 2D and 3D perovskites.[37,38] However, $BZA_2GeBr_4$ shows a lower band gap compared with $PEA_2GeBr_4$, which possess the analogous phase and atomic species to that of $BZA_2GeBr_4$, thus showing a consistent trend with experiments. Calculation of the electronic band structure of the four systems (Fig. 6) shows that all the structures have a direct band gap nature, which is again consistent with the experimental results of the optical measurements (Table 2).

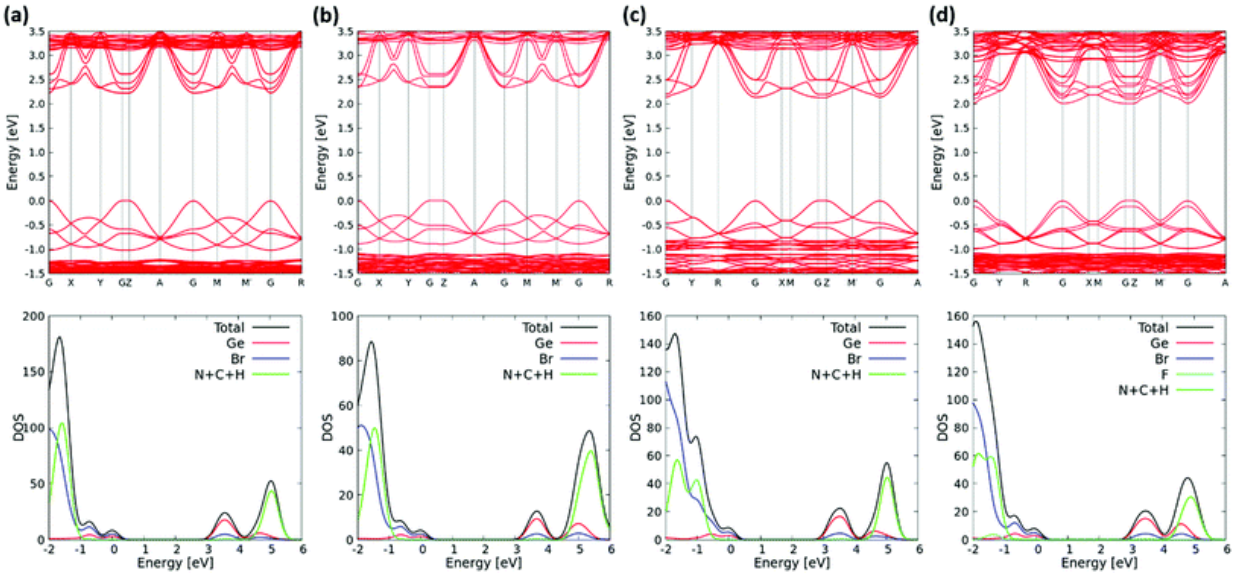


**Fig. 6** Band structure (GGA-PBE level) and DOS (HSE06-SOC level) of (a) $BZA_2GeBr_4$, (b) $PEA_2GeBr_4$, (c) $BrPEA_2GeBr_4$ and (d) $FPEA_2GeBr_4$. The VBM has been set to zero in both the band structure and DOS figures.

**Table 2** Band gaps (eV) for the different structures at the HSE06-SOC level of theory

| Composition | Experiment | Theory |
|---|---|---|
| $BZA_2GeBr_4$ | 2.89 | 3.34 |
| $PEA_2GeBr_4$ | 3.01 | 3.46 |
| $BrPEA_2GeBr_4$ | 2.95 | 3.24 |
| $FPEA_2GeBr_4$ | 2.91 | 3.12 |

Taking together the structural and optical properties, it is possible to discuss their correlation considering the structural distortion of the four samples. We first consider the dependence of $E_g$ and PL with the octahedral elongation $\langle\lambda_{oct}\rangle$ and the bond angle variance ($\sigma_{oct}^2$). These parameters are known to affect the band gap and photoluminescence broadening, with a larger distortion correlating to larger band gaps and broadened PL. Building upon previous studies that show correlations between $\lambda_{oct}$ and $\sigma_{oct}^2$ in Pb-based systems, the values reported in our investigation locate these 2D Ge perovskites in a region of substantially broad PL, accompanied by a high Stokes shift.[5,39] Looking at Fig. 3, it can be seen that $BZA_2GeBr_4$ and $FPEA_2GeBr_4$ lie in a region of the $\lambda_{oct}$*vs.* $\sigma_{oct}^2$ plot where a lower Stokes shift should occur (with respect to the other samples). Indeed, this has been confirmed by PL and TRPL measurements, highlighting also for these two samples a longer $\tau_{average}$ in comparison with $PEA_2GeBr_4$ and $BrPEA_2GeBr_4$. Fig. 7a and b display the trend of the band gaps for the four 2D samples as a function of $\lambda_{oct}$ and $\sigma_{oct}^2$, confirming the correlation but still with the deviation of $BrPEA_2GeBr_4$, which can be ascribed to the peculiar structural disorder found in this sample, and which deserves further study.

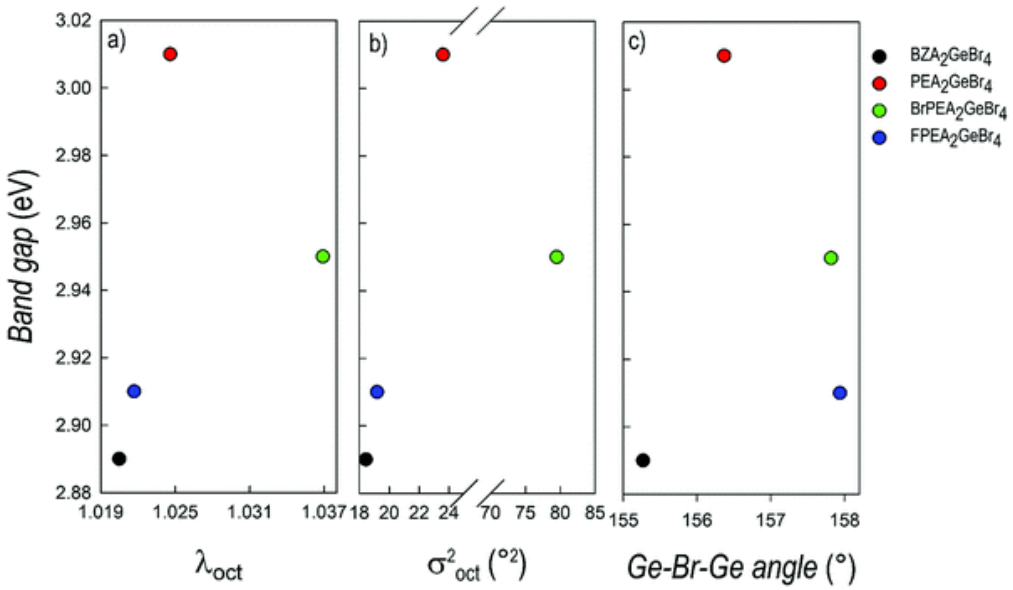


**Fig. 7** Variation of the band gap as a function of the (a) octahedral elongation, (b) angle variance, and (c) Ge–Br–Ge angle for $BZA_2GeBr_4$, $PEA_2GeBr_4$, $BrPEA_2GeBr_4$ and $FPEA_2GeBr_4$.

The other key parameter affecting the band gap is the perovskite layer distortion, with its increase usually related to an increase of the bandgap.[29,40,41] This relationship holds for $PEA_2GeBr_4$, $BrPEA_2GeBr_4$, and $FPEA_2GeBr_4$, whereas $BZA_2GeBr_4$ has the largest deviation from 180° in the Br–Ge–Br angle but also the smallest bandgap (see Fig. 7c). However, this compound shows the least distortion within the octahedra, which is true also for tin- and lead-containing analogues, with a small bandgap (2.4 eV) reported for $BZA_2SnBr_4$, too.[29,31] Thus, this behavior might emerge from the interplay between the two main distortion mechanisms in hybrid perovskites, octahedral and layer distortion, with the former compensating the latter.

Finally, by taking together the present study and previous investigations on $PEA_2SnBr_4$, $BZA_2SnBr_4$, $PEA_2PbBr_4$, and $BZA_2PbBr_4$, some further correlations related to the role of the central atom in 2D metal halide perovskites, for the same organic spacers and halide, can be proposed. Fig. 8 presents the plot of $\lambda_{oct}$ and $\sigma_{oct}^2$ for the six samples, namely $BZA_2BBr_4$ and $PEA_2BBr_4$, B = Pb, Sn, and Ge. In the bottom left part of the plot we find the BZA-containing samples, with Sn and Pb possessing a regular octahedral framework. By replacing BZA with PEA the distortion increases (in particular for the bond angle variance) for $PEA_2PbBr_4$ and $PEA_2SnBr_4$. On the other hand, the two Ge-containing samples show the highest level of distortion (the upper right part of the plot) for both cations, thus bringing to the fore the role of the central atom in the distortion correlation.

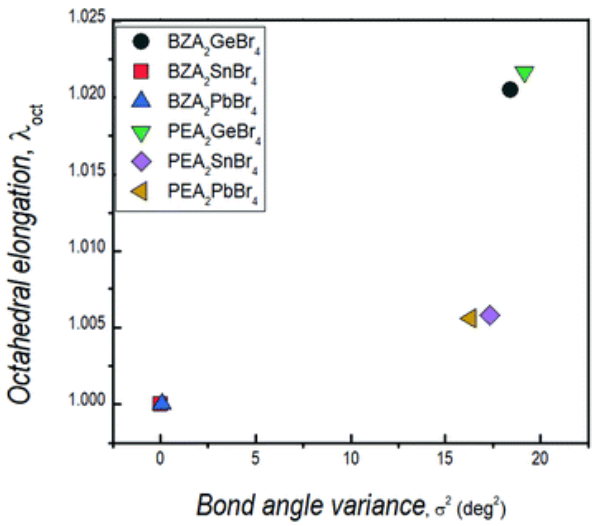


**Fig. 8** Variation of the octahedral elongation *vs.* bond angle variance for $BZA_2BBr_4$ and $PEA_2BBr_4$, B = Pb, Sn, and Ge.

This trend is of interest for the further design of 2D halide perovskites and in particular to look for white-emitting samples. Indeed, the central Ge atom provides, as also highlighted before, a significant degree of octahedral distortion, specifically with respect to $\lambda_{oct}$ and $\sigma_{oct}^2$ and less to the in-plane octahedral angle variation. The first two parameters mostly affect the nature of the emission, providing broadened PL and relevant Stokes shifts, while the angle distortion mostly affects the band gap.[5,39–41] Even if the number of compositionally equivalent 2D metal halide perovskites available to perform correlations is modest so far (in terms of the organic spacer, central atom, and halide), based on the present and previous results we argue that a wise strategy to look for white-emitting 2D perovskites might be to use highly distorting organic spacers, such as 2,2'-(ethylenedioxy)bis(ethylammonium) (EDBE), coupled to Ge as the central atom, which already provides an intrinsically higher level of octahedral distortion with respect to Sn and Pb, but with less pronounced angular distortions affecting the band gap.

## Conclusions

Four novel 2D Ge-based perovskites have been reported, namely $A_2GeBr_4$ with A = PEA, BrPEA, FPEA, and BZA, and characterized in terms of their crystal structure, optical properties, and computational modelling. The role of the different spacers has been demonstrated in terms of variation in the band gap and distortion, as well as Stokes shift and PL decay. Structural distortions in these layered perovskites have been highlighted by correlating the octahedral elongation length ($\lambda_{oct}$), bond angle variance ($\sigma_{oct}^2$), and Ge–Br–Ge angle variation to the mentioned optical properties. In general, some common trends with analogous parameters in Pb- and Sn-based 2D perovskites have been found; however, a peculiar role of Ge in increasing the octahedral distortion is seen in terms of elongation and bond angle variance, although this less in terms of Ge–Br–Ge deviations. $BZA_2GeBr_4$ and $FPEA_2GeBr_4$ were found to lie in a region of low $\lambda_{oct}$ and $\sigma_{oct}^2$, which corresponds to lower band gaps and longer decay times compared with the more distorted $PEA_2GeBr_4$ and $BrPEA_2GeBr_4$. The range of correlations reported in this work for the 2D Ge-based perovskites and, where present, for the analogous Pb- and Sn-counterparts, sheds more light on the relative role of cation-spacer-induced distortion and central atom (intrinsic) distortion on the octahedra framework. Overall, this set of results may help in predicting and designing novel germanium containing perovskites with tailored optical properties by utilizing the distortion level of the inorganic framework induced by the organic spacer, thus expanding the actual knowledge on 2D halide perovskites.

## Conflicts of interest

There are no conflicts to declare.

## Acknowledgements

A.M. and F. D. A. acknowledge the European Union's Horizon 2020 research and innovation programme under Grant Agreement No. 764047 of the ESPRESSO project. The Ministero dell'Istruzione dell'Università e della Ricerca (MIUR) and Università degli Studi di Perugia are acknowledged for financial support through the program "Dipartimenti di Eccellenza 2018–2022" (Grant AMIS) to F. D. A. Both M. M. and L. M. thank the "Fiorenzo Mazzi Experimental Mineralogy laboratory" (University of Pavia) and CRIST "Centro di Cristallografia Strutturale" (University of Florence) for support in the data collection.

## References

1. X. Li , J. M. Hoffman and M. G. Kanatzidis , *Chem. Rev.*, 2021, **121** , 2230 —2291
2. L. Mao , C. C. Stoumpos and M. G. Kanatzidis , *J. Am. Chem. Soc.*, 2019, **141** , 1171 —1190
3. B. Saparov and D. B. Mitzi , *Chem. Rev.*, 2016, **116** , 4558 —4596
4. M. D. Smith , E. J. Crace , A. Jaffe and H. I. Karunadasa , *Annu. Rev. Mater. Res.*, 2018, **48** , 111 —136
5. D. Cortecchia , S. Neutzner , A. R. Srimath Kandada , E. Mosconi , D. Meggiolaro , F. De Angelis , C. Soci and A. Petrozza , *J. Am. Chem. Soc.*, 2017, **139** , 39 —42
6. J. L. Knutson , J. D. Martin and D. B. Mitzi , *Inorg. Chem.*, 2005, **44** , 4699 —4705
7. Z. Xu , D. B. Mitzi , C. D. Dimitrakopoulos and K. R. Maxcy , *Inorg. Chem.*, 2003, **42** , 2031 —2039
8. M.-H. Tremblay , J. Bacsa , B. Zhao , F. Pulvirenti , S. Barlow and S. R. Marder , *Chem. Mater.*, 2019, **31** , 6145 —6153
9. P.-X. Wang , A. M. Najarian , Z. Hao , A. Johnston , O. Voznyy , S. Hoogland and E. H. Sargent , *J. Phys. Chem. Lett.*, 2020, **11** , 10144 —10149

10. A. Krishna , S. Gottis , M. K. Nazeeruddin and F. Sauvage , *Adv. Funct. Mater.*, 2019, **29** , 1806482

11. L. Zhang , Y. Liu , Z. Yang and S. (Frank) Liu , *J. Energy Chem.*, 2019, **37** , 97 —110

12. M. Seitz , A. J. Magdaleno , N. Alcázar-Cano , M. Meléndez , T. J. Lubbers , S. W. Walraven , S. Pakdel , E. Prada , R. Delgado-Buscalioni and F. Prins , *Nat. Commun.*, 2020, **11** , 2035

13. M. I. Saidaminov , O. F. Mohammed and O. M. Bakr , *ACS Energy Lett.*, 2017, **2** , 889 —896

14. H.-P. Wang , S. Li , X. Liu , Z. Shi , X. Fang and J.-H. He , *Adv. Mater.*, 2021, **33** , 2003309

15. R. Dong , C. Lan , F. Li , S. Yip and J. C. Ho , *Nanoscale Horiz.*, 2019, **4** , 1342 —1352

16. C. Fang , H. Wang , Z. Shen , H. Shen , S. Wang , J. Ma , J. Wang , H. Luo and D. Li , *ACS Appl. Mater. Interfaces*, 2019, **11** , 8419 —8427

17. L. Gao , J. You and S. (Frank) Liu , *J. Energy Chem.*, 2021, **57** , 69 —82

18. A. M. Sanni and A. S. Rury , *J. Phys. Chem. Lett.*, 2021, **12** , 101 —110

19. W. Paritmongkol , E. R. Powers , N. S. Dahod and W. A. Tisdale , *J. Phys. Chem. Lett.*, 2020, **11** , 8565 —8572

20. J. Yin , R. Naphade , L. Gutiérrez Arzaluz , J.-L. Brédas , O. M. Bakr and O. F. Mohammed , *ACS Energy Lett.*, 2020, **5** , 2149 —2155

21. R. Gautier , M. Paris and F. Massuyeau , *J. Am. Chem. Soc.*, 2019, **141** , 12619 —12623

22. M. D. Smith , B. A. Connor and H. I. Karunadasa , *Chem. Rev.*, 2019, **119** , 3104 —3139

23. A. Abate *Joule*, 2017, **1** , 659 —664

24. F. De Angelis *ACS Energy Lett.*, 2021, **6** , 1586 —1587

25. X. Chang , D. Marongiu , V. Sarritzu , N. Sestu , Q. Wang , S. Lai , A. Mattoni , A. Filippetti , F. Congiu , A. G. Lehmann , F. Quochi , M. Saba , A. Mura and G. Bongiovanni , *Adv. Funct. Mater.*, 2019, **29** , 1903528

26. P. Cheng , T. Wu , J. Liu , W.-Q. Deng and K. Han , *J. Phys. Chem. Lett.*, 2018, **9** , 2518 —2522

27. P. Cheng , T. Wu , J. Zhang , Y. Li , J. Liu , L. Jiang , X. Mao , R.-F. Lu , W.-Q. Deng and K. Han , *J. Phys. Chem. Lett.*, 2017, **8** , 4402 —4406

28. D. B. Mitzi *J. Chem. Soc., Dalton Trans.*, 2001, 1 —12

29. K. Du , Q. Tu , X. Zhang , Q. Han , J. Liu , S. Zauscher and D. B. Mitzi , *Inorg. Chem.*, 2017, **56** , 9291 —9302

30. K. Robinson , G. V. Gibbs and P. H. Ribbe , *Science*, 1971, **172** , 567 —570

31. A. Pisanu , M. Coduri , M. Morana , Y. O. Ciftci , A. Rizzo , A. Listorti , M. Gaboardi , L. Bindi , V. I. E. Queloz , C. Milanese , G. Grancini and L. Malavasi , *J. Mater. Chem. A*, 2020, **8** , 1875 —1886

32. G. S. Lorena , H. Hasegawa , Y. Takahashi , J. Harada and T. Inabe , *Chem. Lett.*, 2014, **43** , 1535 —1537

33. J. R. Lakowicz *Principles of fluorescence spectroscopy* , Springer, New York, NY, 2010

34. J.-C. Blancon , A. V. Stier , H. Tsai , W. Nie , C. C. Stoumpos , B. Traoré , L. Pedesseau , M. Kepenekian , F. Katsutani , G. T. Noe , J. Kono , S. Tretiak , S. A. Crooker , C. Katan , M. G. Kanatzidis , J. J. Crochet , J. Even and A. D. Mohite , *Nat. Commun.*, 2018, **9** , 2254

35. Y. Gao , M. Zhang , X. Zhang and G. Lu , *J. Phys. Chem. Lett.*, 2019, **10** , 3820 —3827

36. F. Zhang , D. H. Kim , H. Lu , J.-S. Park , B. W. Larson , J. Hu , L. Gao , C. Xiao , O. G. Reid , X. Chen , Q. Zhao , P. F. Ndione , J. J. Berry , W. You , A. Walsh , M. C. Beard and K. Zhu , *J. Am. Chem. Soc.*, 2019, **141** , 5972 —5979

37. M. Coduri , T. A. Strobel , M. Szafrański , A. Katrusiak , A. Mahata , F. Cova , S. Bonomi , E. Mosconi , F. De Angelis and L. Malavasi , *J. Phys. Chem. Lett.*, 2019, **10** , 7398 —7405

38. C. Gao , R. Li , Y. Li , R. Wang , M. Wang , Z. Gan , L. Bai , Y. Liu , K. Zhao , S. F. Liu , Y. Cheng and W. Huang , *J. Phys. Chem. Lett.*, 2019, **10** , 5687 —5693

39. D. Cortecchia , J. Yin , A. Petrozza and C. Soci , *J. Mater. Chem. C*, 2019, **7** , 4956 —4969

40. J. L. Knutson , J. D. Martin and D. B. Mitzi , *Inorg. Chem.*, 2005, **44** , 4699 —4705

41. P.-X. Wang , A. M. Najarian , Z. Hao , A. Johnston , O. Voznyy , S. Hoogland and E. H. Sargent , *J. Phys. Chem. Lett.*, 2020, **11** , 10144 —10149

42. R. Chiara , M. Morana and L. Malavasi , *ChemPlusChem*, 2021, **86** , 879 —888